

Optics Design and Performance of an Ultra-Low Emittance Damping Ring for CLIC

Maxim Korostelev

CLIC damping ring lattice

Injection and extraction

Non-Linear Optimization Of The CLIC Damping Ring Lattice

SR power and absorption

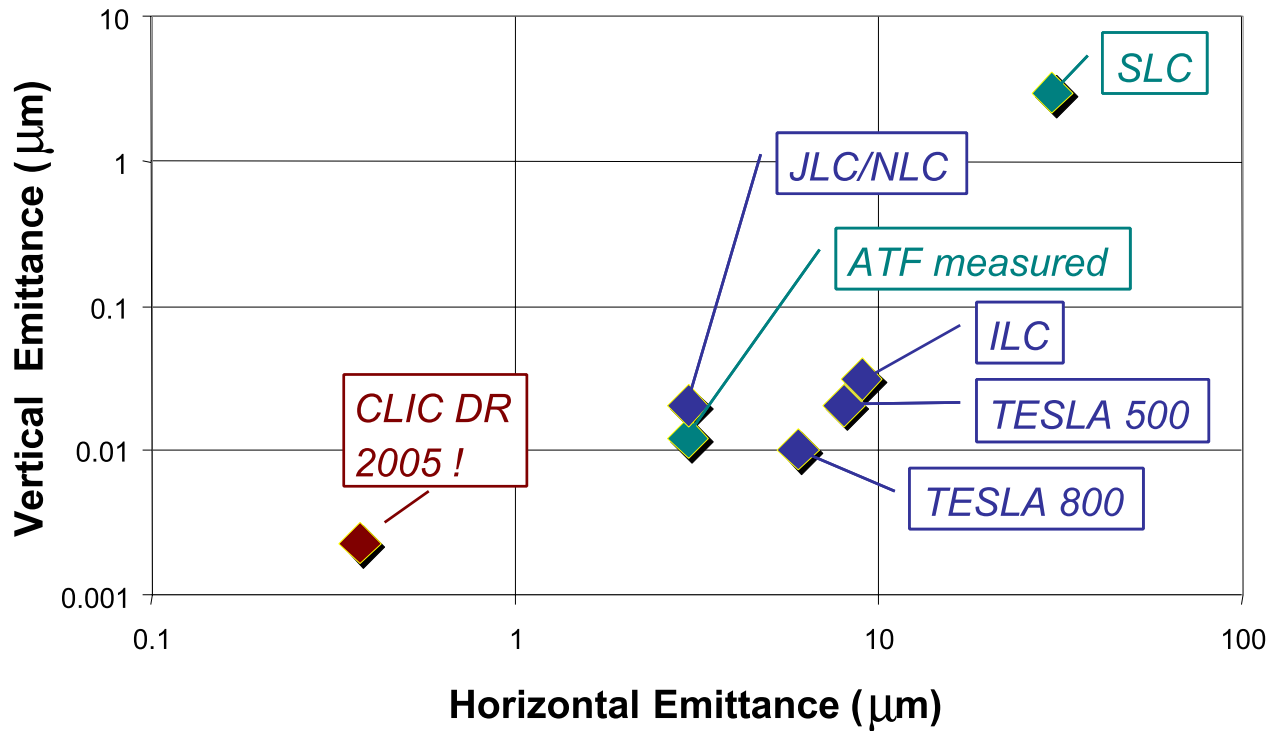
Nonlinearities induced by the short period NbFeB permanent wiggler

Tolerances for Alignment Errors.

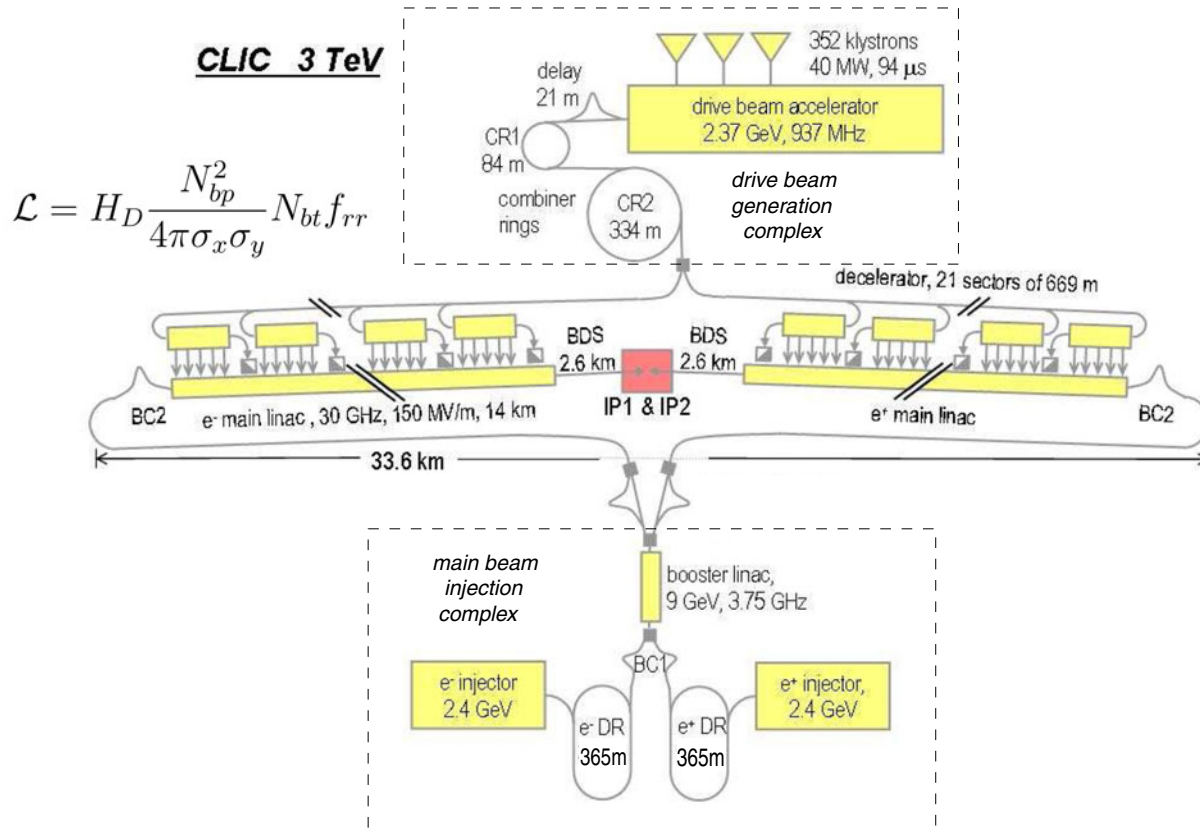
Correction of Vertical Dispersion and Betatron Coupling.

Collective Effects in the CLIC Damping Rings

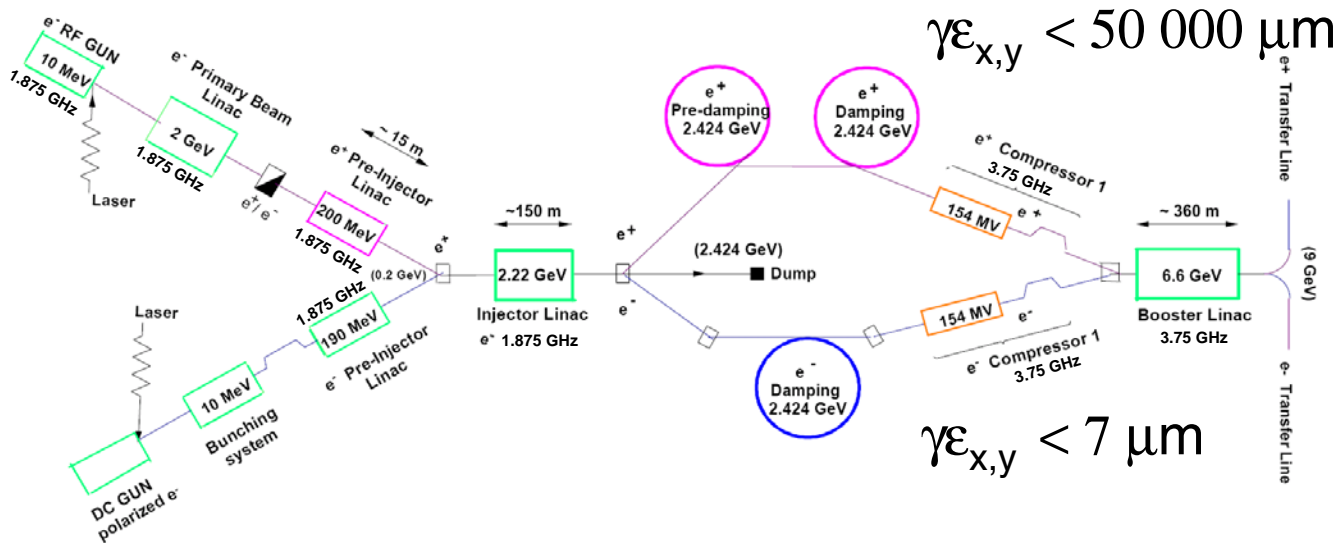
Normalised r.m.s. Emittances at Damping Ring Extraction



Schematic Overall Layout of the CLIC Complex



Main Beam Injector Layout



Expected parameters of beam injected into CLIC positron main damping ring

Parameter	Symbol	Value
Horizontal beam emittance at injection	$\gamma\epsilon_x$	63 μm
Vertical beam emittance at injection	$\gamma\epsilon_y$	1.5 μm
RMS bunch length at injection	σ_s	10 mm
RMS relative energy spread at injection	σ_δ	0.5 %

The design of the NLC positron pre-damping ring* with some modification could be adopted to the CLIC injection complex.

*

I. Reichel, A. Wolski, "A reduced emittance lattice for the NLC positron pre-damping ring," Proceedings of EPAC 2004, Lucerne, Switzerland.

Beam parameters at the interaction point of CLIC

Parameter	Symbol	Value
Bunch population	N_{bp}	2.56×10^9
No. of bunches per machine pulse	N_{bt}	220
Repetition frequency (No. of machine pulses per second)	f_{rr}	150 Hz
Bunch spacing	τ_b	8 cm
Horizontal emittance at IP	$\gamma\epsilon_x$	660 nm
Vertical emittance at IP	$\gamma\epsilon_y$	10 nm
RMS bunch length at IP	σ_s	30.8 μm

final focus system,
collimation system,
and bunch compressors

longitudinal
compression

subsequent
transportation to
the main linac

acceleration
in the main linac

collimation and
strong focusing in
the BDS

Beam parameters required for the CLIC main damping ring

Parameter	Symbol	Value
Bunch population	N_{bp}	2.56×10^9
No. of bunches per machine pulse	N_{bt}	220
Repetition frequency (No. of machine pulses per second)	f_{rr}	150 Hz
Horizontal beam emittance at extraction	$\gamma\epsilon_x$	450 nm
Vertical beam emittance at extraction	$\gamma\epsilon_y$	3 nm
Longitudinal beam emittance at extraction	$\gamma\sigma_s\sigma_\delta m_0 c^2$	< 5000 eVm

layout of the CLIC damping ring



25 m

The minimum emittance

$$\beta_m^* = \frac{L}{2\sqrt{15}} \quad D_m^* = \frac{L\theta}{24}$$

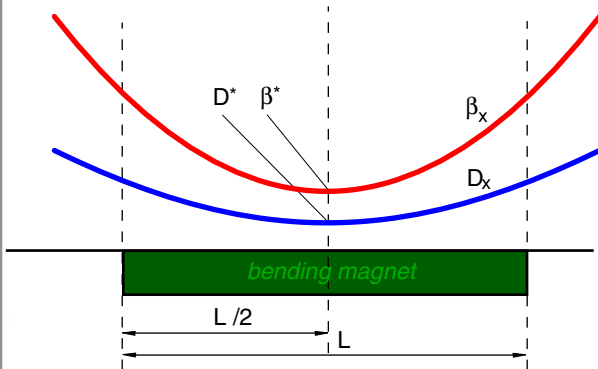
$$\alpha_m^* = 0 \quad D_m^{*'} = 0$$

$$\gamma \epsilon_{x0m} = \frac{C_q \gamma^3}{J_x} \frac{\theta^3}{12\sqrt{15}}$$

$$\beta_r \equiv \beta^* / \beta_m^* \quad D_r \equiv D^* / D_m^*$$

$$\epsilon_{x0} \equiv \epsilon_r \epsilon_{x0m}$$

$$\epsilon_r = \frac{5}{8} \frac{D_r}{\beta_r} [D_r - 2] + \frac{9}{2} \left[\frac{1}{4\beta_r} + \frac{\beta_r}{9} \right]$$



The horizontal dispersion D_x and betatron function β_x have *optical symmetry with respect to the bend center*, i.e. $D_x^{*'} = 0$ and $\alpha_x^* = 0$ at the middle of the bending magnet.

High brilliance lattice types

Double Focusing Achromat (DFA)

ESRF, APS, ELETTRA, SUPERACO, SOLEIL

+ large dispersion between two magnets => does not need too strong sextupole magnets

- the beta functions in the insertion region are coupled by a choice of the phase advance

Triplet Achromat Lattice (TAL)

storage ring ACO at Orsay

+ compact cell

- emittance depends on the value of the hor. betatron function in the insertion region

Triplet Bend Achromat (TBA)

ALADDIN, BESSY, ALS in Berkeley, SRRC in Taiwan, and PLS. It was also proposed for the DIAMOND project

+ easy to vary a phase advance over the cell

- needs strong sextupole magnets

Theoretical minimum emittance lattice (TME)

+ compact cell, gives smallest emittance

- needs strong sextupoles

$$\frac{\epsilon_{\text{DFA}}^{\text{min}}}{\epsilon_{\text{TME}}^{\text{min}}} = 3$$

$$\frac{\epsilon_{\text{TAL}}^{\text{min}}}{\epsilon_{\text{TME}}^{\text{min}}} = 12$$

$$\frac{\epsilon_{\text{TBA}}^{\text{min}}}{\epsilon_{\text{TME}}^{\text{min}}} = 7/3$$

energy

As CLIC will operate with polarized beams, the damping ring must maintain a high spin polarization. Therefore, the ring energy should be chosen so that the spin tune is a half integer to stay away from the strong integer spin resonance. This constrains the ring energy to

$$E = \frac{(n + 1/2)m_0c^2}{a} \implies \dots 1.54, 1.98, 2.42, 2.86 \dots [\text{GeV}]$$

Here, $a = 1.16 \times 10^{-3}$ is the anomalous magnetic moment of the electron, n is an integer number.

Intrabeam scattering

The horizontal ε_x , vertical ε_y and longitudinal ε_t emittances evolve with time according to a set of three differential equations:

$$\dot{\varepsilon}_x = -\frac{2}{\tau_x}(\varepsilon_x - \varepsilon_{x0}) + \frac{2\varepsilon_x}{T_x(\varepsilon_x, \varepsilon_y, \varepsilon_t)} \quad (1)$$

$$\dot{\varepsilon}_y = -\frac{2}{\tau_y}(\varepsilon_y - \varepsilon_{y0}) + \frac{2\varepsilon_y}{T_y(\varepsilon_x, \varepsilon_y, \varepsilon_t)} \quad (2)$$

$$\dot{\varepsilon}_t = -\frac{2}{\tau_t}(\varepsilon_t - \varepsilon_{t0}) + \frac{2\varepsilon_t}{T_t(\varepsilon_x, \varepsilon_y, \varepsilon_t)} \quad (3)$$

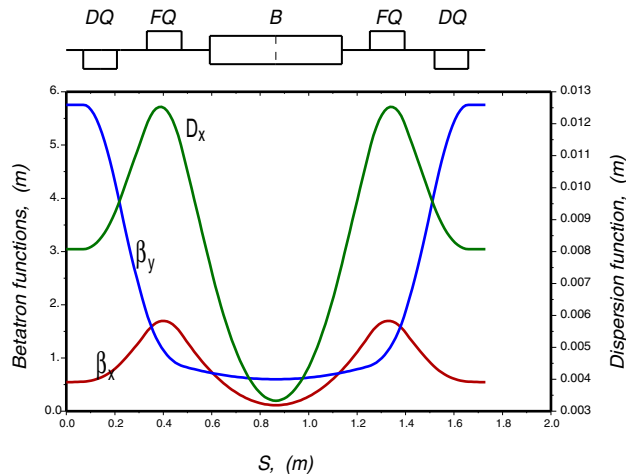
where τ_x, τ_y, τ_t are the radiation damping times of the betatron (xy) and synchrotron (t) oscillations respectively. $\varepsilon_{x0}, \varepsilon_{y0}, \varepsilon_{t0}$ are equilibrium emittances determined by radiation damping and quantum excitation in the absence of IBS and $T_\mu(\varepsilon_x, \varepsilon_y, \varepsilon_t)$, $\mu \in \{x, y, t\}$ are intrabeam scattering growth times which are non-linear functions of emittances.

The equilibrium emittances follow from equation

$$\dot{\varepsilon}_x = \dot{\varepsilon}_y = \dot{\varepsilon}_t = 0$$

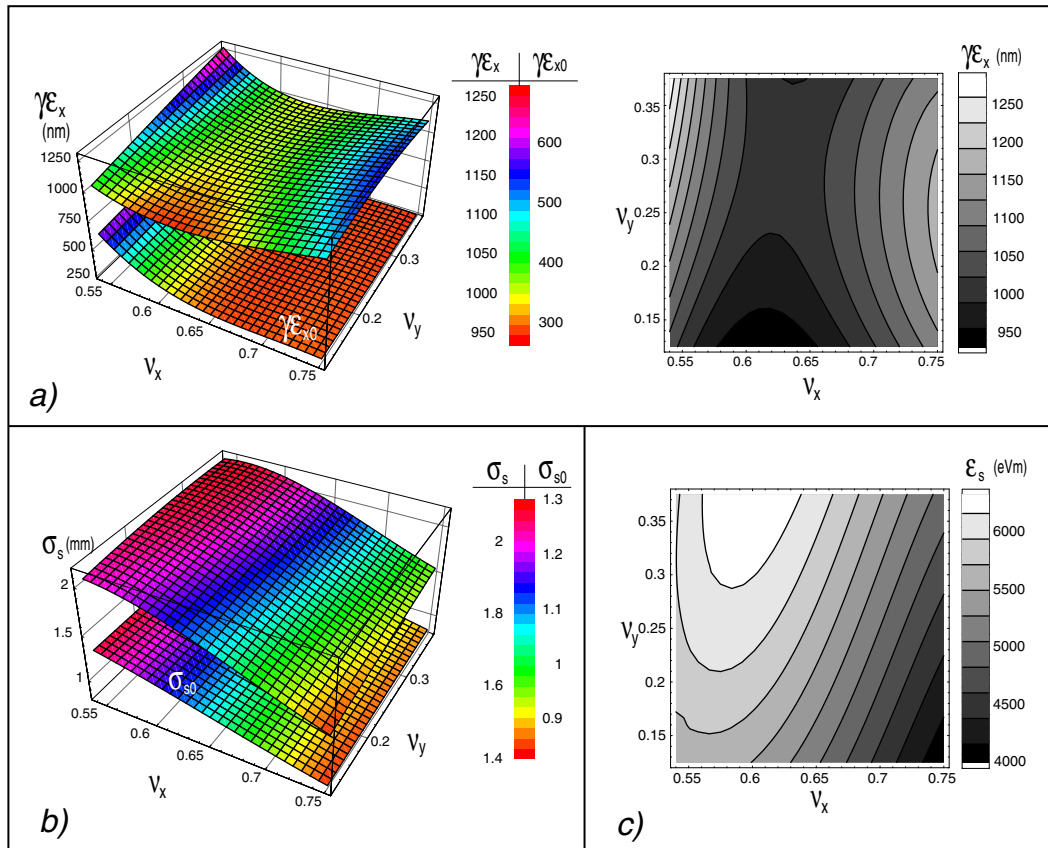
TME cell design for the CLIC damping ring

The lattice functions along the TME cell.

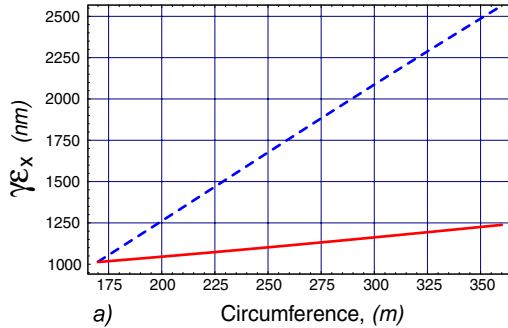


The parameters of the $\nu_x = 0.584$, $\nu_y = 0.25$ TME cell

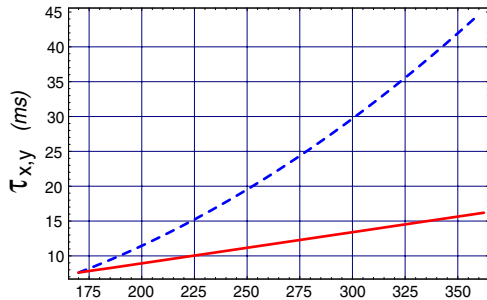
Energy	2.42 GeV
Field of the bending magnet, B_a	0.932 T
Length of the bending magnet	0.545 m
Bending angle	$2\pi/100$
Bending radius	8.67 m
Length of the cell, L_{TME}	1.73 m
Horizontal phase advance, μ_x	210°
Vertical phase advance, μ_y	90°
Emittance detuning factor, ϵ_r	1.8
Horizontal chromaticity, $\partial\nu_x/\partial\delta$	-0.84
Vertical chromaticity, $\partial\nu_y/\partial\delta$	-1.18
Average horizontal beta function, $\langle\beta_x\rangle$	0.847 m
Average vertical beta function, $\langle\beta_y\rangle$	2.22 m
Average horizontal dispersion, $\langle D_x\rangle$	0.0085 m
Relative horizontal beta function, $\beta_r = \beta^*/\beta_m^*$	$0.113/0.07 = 1.6$
Relative horizontal dispersion, $D_r = D^*/D_m^*$	$0.00333/0.00143 = 2.33$



The comparison between equilibrium beam parameters computed with IBS and without IBS (denoted by "0") for 100 TME cells



a) Circumference, (m)



b) Circumference, (m)

The parameters of the ring consisting of 100 TME cells.

Energy, E	2.42 GeV
Ring circumference, C	173 m
Horizontal emittance w/o IBS, $\gamma\epsilon_{x0}$	394 nm
Horizontal emittance with IBS, $\gamma\epsilon_x$	1026 nm (1100 nm)*
Horizontal/vertical damping time, $\tau_{x,y}$	7.94 ms
Horizontal IBS growth time, T_x	12.3 ms (11.8 ms)*
Longitudinal IBS growth time, T_p	9.7 ms (9.25 ms)*
RMS energy spread w/o IBS, σ_δ	7.05×10^{-4}
RMS energy spread with IBS, σ_δ	12×10^{-4} (12.3×10^{-4})*
Energy loss per turn, U_0	0.353 MeV/turn
RF frequency, f_{rf}	1875 MHz
Momentum compaction factor, α_p	1.726×10^{-4}
RMS bunch length (at $V_{rf} = 700$ kV) w/o IBS, σ_s	1.2 mm
RMS bunch length (at $V_{rf} = 700$ kV) with IBS, σ_s	2.1 mm (2.15 mm)*
Longitudinal emittance w/o IBS, $\gamma\sigma_s\sigma_\delta m_0c^2$	2100 eV m
Longitudinal emittance with IBS, $\gamma\sigma_s\sigma_\delta m_0c^2$	6045 eV m (6447 eV m)*

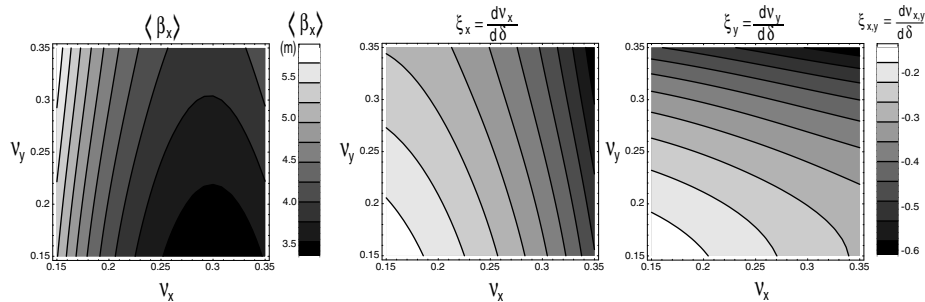
* Note that the IBS was computed according to modified-Piwinski method (Sec. 3.5). The values pointed out in the brackets and marked by symbol "*" were computed by Bane's high energy approximation method (Sec. 3.3).

Note that the parameters in this table were computed for the emittance ratio $\epsilon_{y0}/\epsilon_{x0} = 0.0063$.

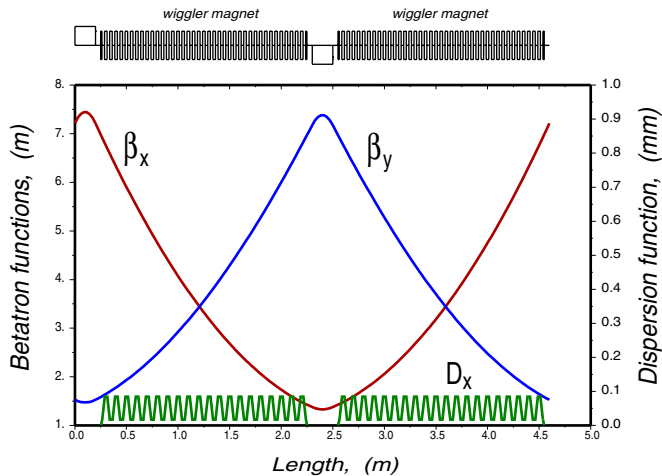
394 nm ~~---~~ IBS ~~---~~ 1026 nm

a) The growth of horizontal equilibrium emittance in the presence of IBS as a function of the ring circumference; b) the growth of the transverse damping time $\tau_{x,y}$ with circumference. The dashed lines on both plots correspond to the case when the length of bending magnet is increased together with the length of drift space. The solid lines correspond to the case when the length of bending magnet is constant and equal to 0.545 m (only drift spaces are changed). The ring consisting of 100 TME cells without wigglers.

Lattice design of the wiggler FODO cell



The average horizontal beta function $\langle \beta_x \rangle$ and chromaticities ξ_x , ξ_y as a functions of the horizontal and vertical phase advance ν_x , ν_y of the FODO cell with length of 4.6 m.



The lattice function of the

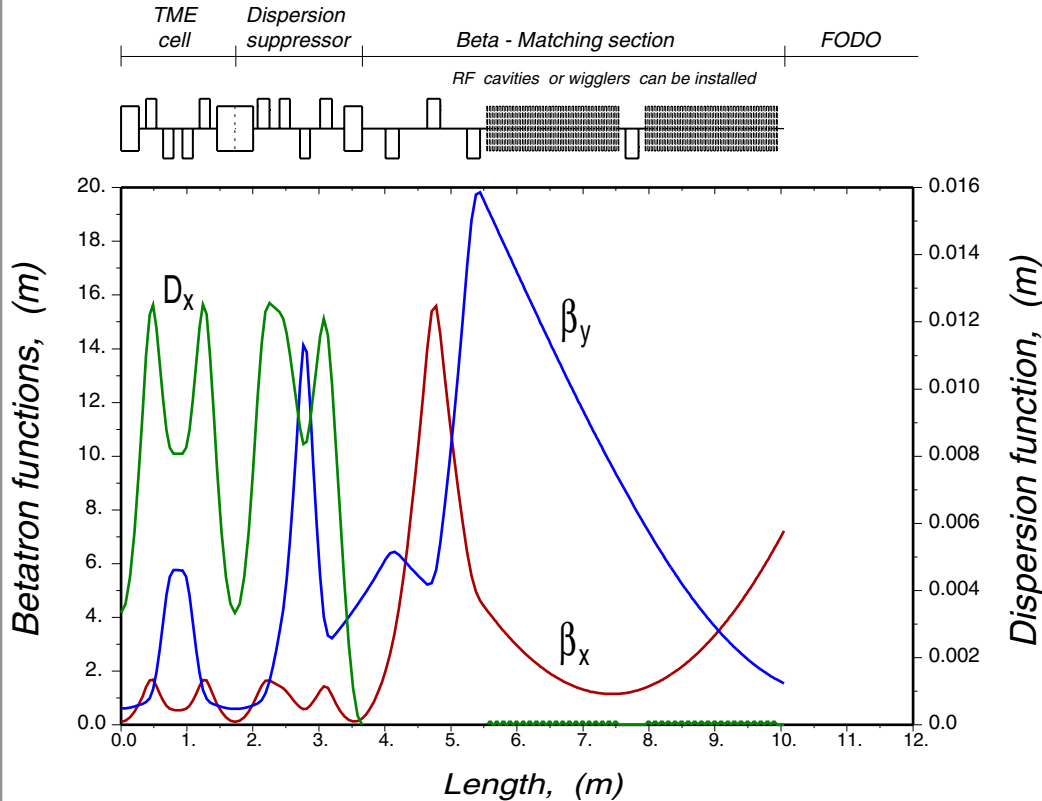
$$\mu_x = 0.26 \times 2\pi = 93.6^\circ$$

$$\mu_y = 0.24 \times 2\pi = 86.4^\circ$$

FODO cell with two wiggler magnets

$$\lambda_w = 10 \text{ cm}, B_w = 1.7 \text{ T} \text{ and } L_{ID} = 2 \text{ m}$$

Lattice design of the dispersion suppressor and beta-matching section



it is possible to vary the horizontal and vertical phase advance between the last TME cell and the first FODO cell in the range of

$$\mu_x = (1.16 \pm 0.1) \times 2\pi$$

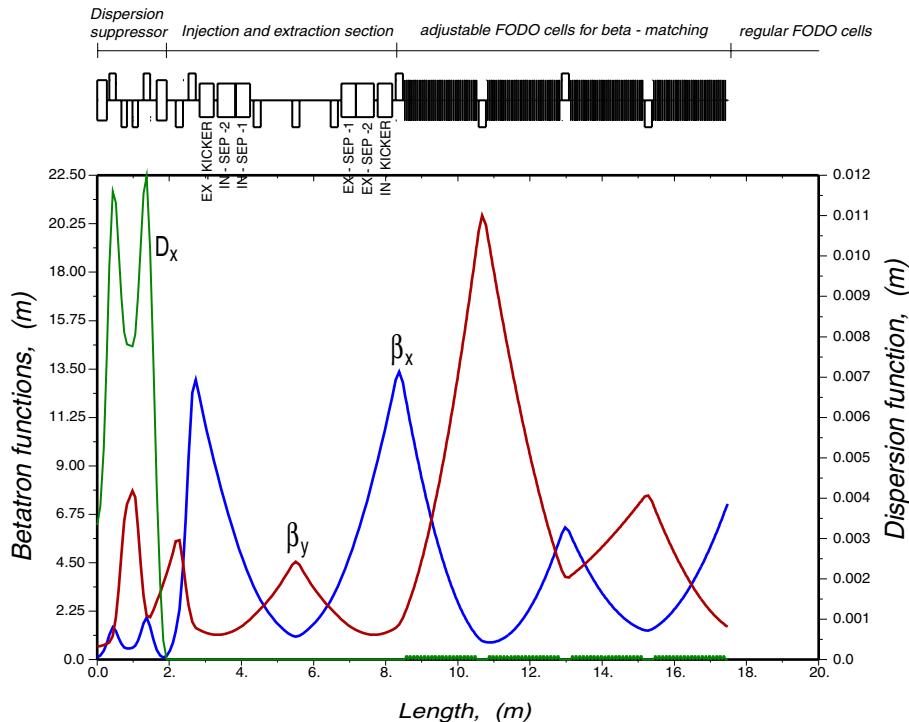
$$\mu_y = (0.34 \pm 0.12) \times 2\pi$$

if the phase advances per FODO cell with wigglers ($0 < Bw < 2.52$ T) are in the range of

$$\mu_x = (0.26 \pm 0.01) \times 2\pi$$

$$\mu_y = (0.24 \pm 0.01) \times 2\pi$$

Lattice design of the injection/extraction region



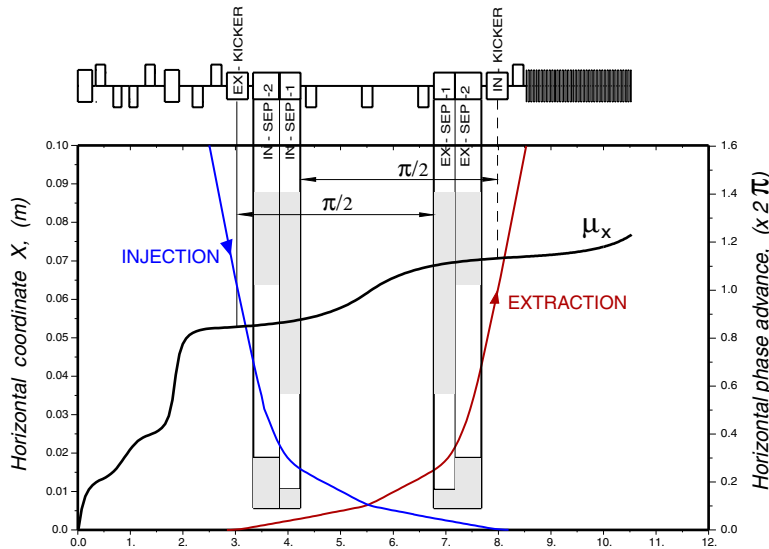
The length of the injection/extraction section is exactly equal to the length of the beta-matching section

The kickers IN-KICKER and EX-KICKER are placed just up-stream and down-stream, respectively, of the F-quadrupoles where the beta function is largest. The phase advance between IN-SEP and IN-KICKER is $\pi/2$. The phase advance between EX-KICKER and EX-SEP is the same.

The horizontal and vertical phase advance through the dispersion suppressor, injection/extraction

section and two adjustable FODO cells are equal to $\mu = 1.68 \times 2\pi$ and $0.82 \times 2\pi$. Moreover, the horizontal and vertical phase advances through the beta-matching section together with dispersion suppressor and two regular FODO cells are identical.

The injected and extracted beam trajectories through the septum



Parameters of the septum magnets

Parameter	Septum -SEP-1	Septum -SEP-2
Effective length	0.4018 m	0.5018 m
Bending angle	13 mrad	42 mrad
Field integral	0.105 T·m	0.339 T·m
Blade thickness	5 mm	13 mm
Type	DC	DC

Parameters of both kickers

Parameter	Value
Rise time	≤ 25 ns
Fall time	≤ 25 ns
Flat top	142 ns
Repetition rate	150 Hz
Beam energy	2.42 GeV
Effective length	0.4 m
Angular deflection	2.45 mrad
Field	500 Gauss
Beta at kicker	10.7 m
Core material	Ferrite TDK
Injection kicker tolerance	$\pm 1.44 \times 10^{-3}$
Extraction kicker tolerance	$\pm 1.5 \times 10^{-4}$

The design parameters of the septum magnet are based on the septum design developed for the NLC damping ring¹.

Two bunch trains 110×2 with a gap of 25.6 ns are injected simultaneously during one pulse

The kicker must provide a flat top of 142 ns with rise & fall times shorter than 25 ns.

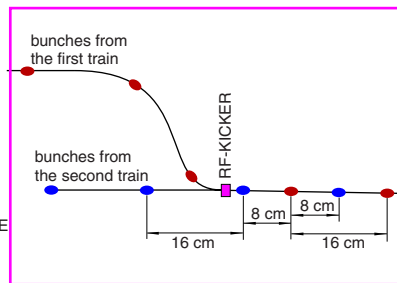
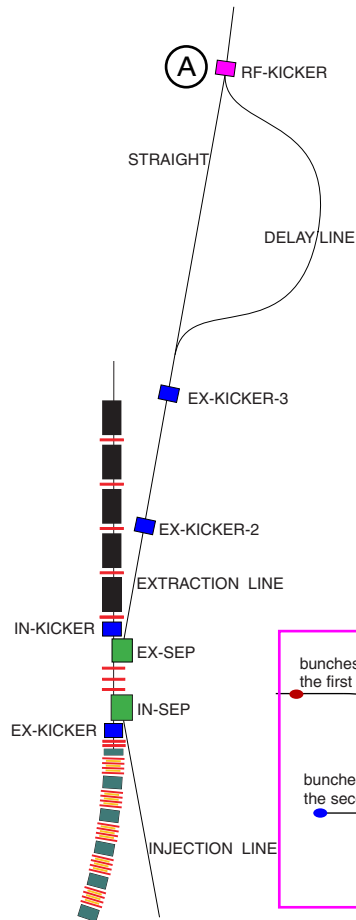
¹ http://www-project.slac.stanford.edu/lc/local/notes/dr/mag_cs.pdf

Injection and extraction scenario

A noteworthy feature of the extraction scheme for the positron (electron) CLIC damping ring

two trains with 110 bunches separated by 16 cm, are extracted simultaneously and need to be combined using a subsequent delay line and RF deflector.

The advantage of two times larger bunch spacing in the damping ring (16 cm) compared with the main linac (8 cm)



(A)

1. alleviates the impact of electron-cloud and fast-ion instabilities,

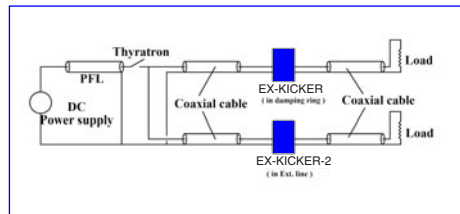
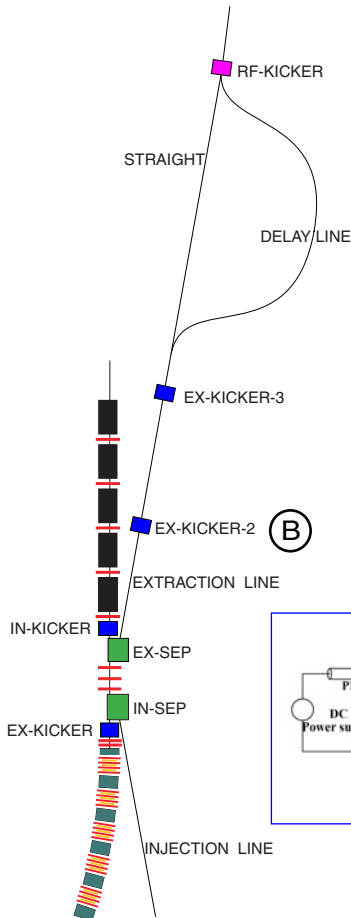
2. allows for a lower RF frequency in the damping ring

$$110 \times 2 \Rightarrow 220$$

Double kicker system

it is important that the extraction kicker has a very small jitter which refers not only to the uniformity of the pulsed magnetic field but also to its pulse-to-pulse stability.

The system uses two identical kicker magnets separated by the phase advance of π . The first kicker EX-KICKER is placed in the damping ring and the second kicker EXKICKER-2 for jitter compensation in the extraction line. Both kickers have a common pulse power supply and produce a kick in the horizontal plane.



If both kickers have a kick angle variation $\Delta\theta_1$ and $\Delta\theta_2$, then the co-ordinates at the exit of the second kicker can be written as

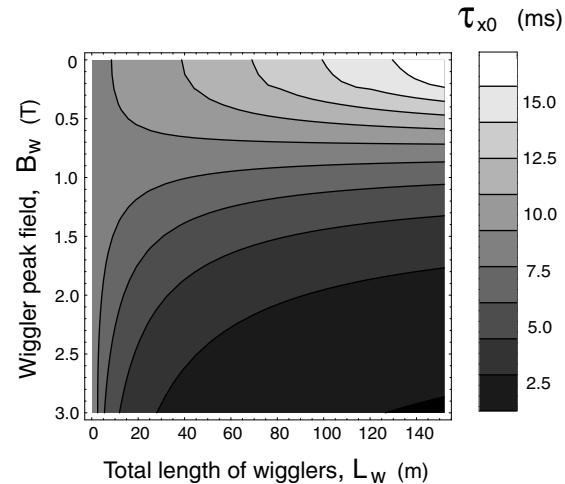
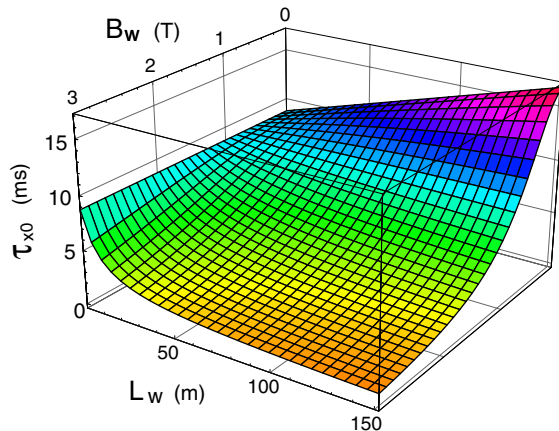
$$x = 0, \quad x' = -\sqrt{\frac{\beta_1}{\beta_2}} \Delta\theta_1 + \Delta\theta_2$$

(B) since the phase advance between the two kickers is π If the two kickers are not identical, compensation also can be achieved by adjusting the β_2 function.

Two Straight Sections with Wigglers

$$\tau_x = \frac{2E_0 T_0}{J_x U_0} = \frac{3(B\rho)C}{2\pi r_0 c \gamma^3 B_a (J_{xa} + F_w)}$$

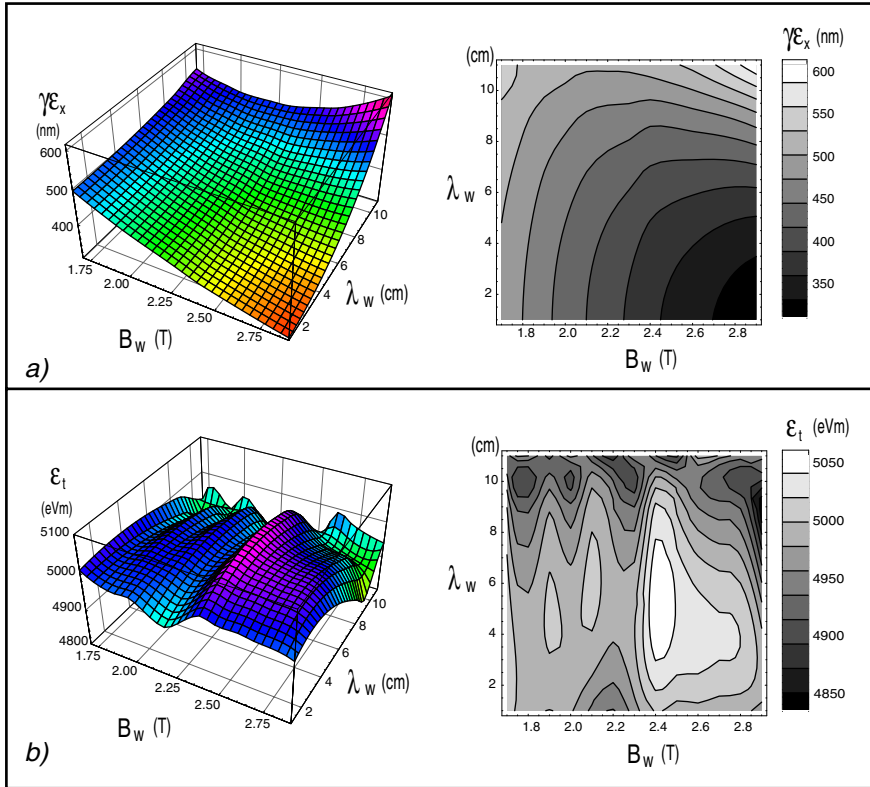
$$F_w \equiv \frac{I_{2w}}{I_{2a}} = \frac{L_w B_w^2}{4\pi(B\rho)B_a}$$



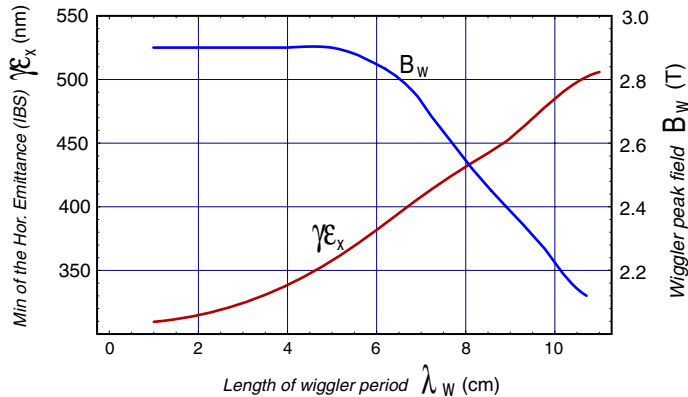
Horizontal damping time τ_{x0} as a function of the total length L_w of the wigglers and the peak field B_w of the wigglers.

the length L_w needed to provide $\tau_{x0} = 3.0$ ms for the wiggler field 1.7 T, 2.0 T, 2.52 T is 146 m, 76 m and 38 m, respectively.

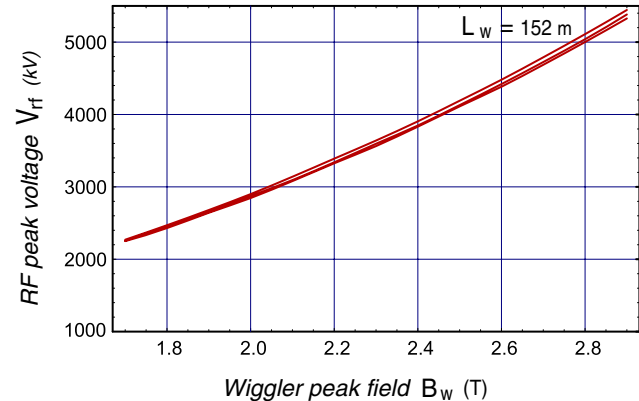
Impact of the IBS effect



Horizontal equilibrium emittances γE_x (figure - a) and longitudinal emittance E_t (figure - c) as a function of the wiggler field B_w and wiggler period λ_w computed with the effect of IBS at the fixed wiggler length $L_w = 152$ m.



The minimum horizontal emittance $\gamma\epsilon_x(\lambda_W)$ (red curves) for the optimal value of the wiggler field B_W (blue curves) at the fixed value of wiggler period λ_W . The solid curves refer to $L_W = 152$ m.



The change of RF peak voltage with the wiggler peak field required to maintain the longitudinal emittance near the value of 5000 eVm. For a given L_W , the three curves refer to wiggler period length of 1, 6 and 11 cm, from top to bottom respectively

Tentative design of Nd-B-Fe hybrid permanent wiggler magnet:

$$\lambda_W = 10 \text{ (cm)} \quad B_W = 1.7 \text{ (T)} \quad L_{ID} = 2 \text{ (m)}$$

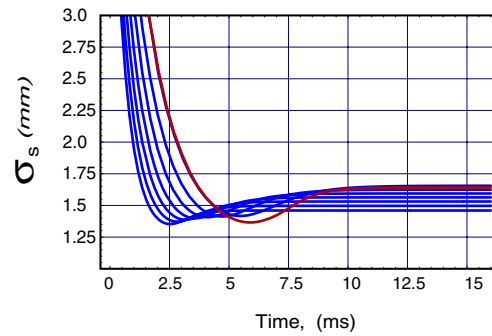
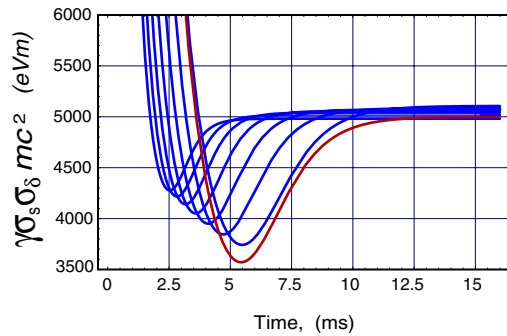
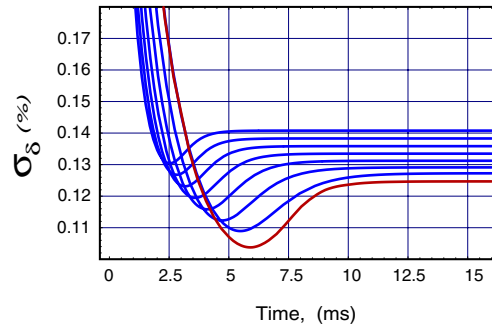
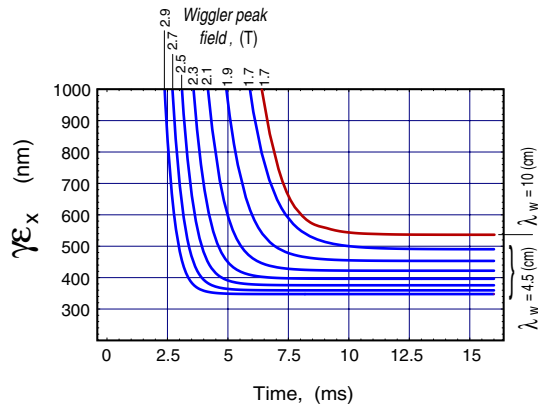
Alternative variant, a Nb₃Sn superconducting wiggler magnet with parameters in the range of 4 cm < λ_W < 5 cm and 2.25T < B_w < 3.05 T

20 mm (pole gap) – 2x1 mm (He wall) – 2x2 mm (safety vacuum)
- 2x1 mm (N wall screen) = 12 mm (beam aperture).

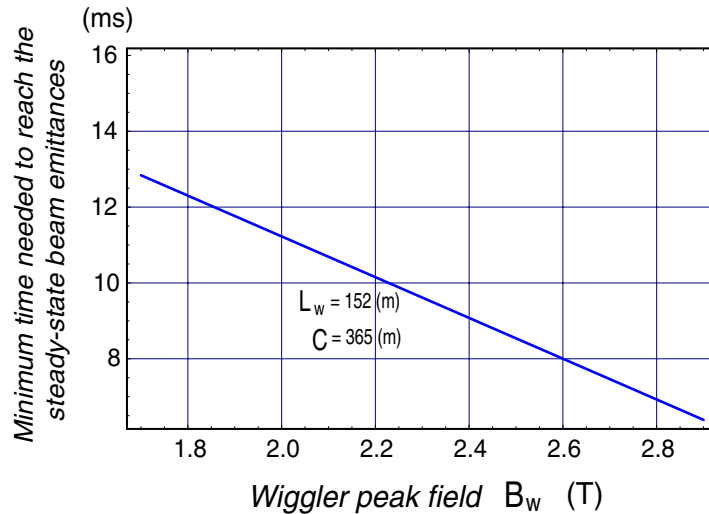
	λ_w (mm)	Iw (kA-t)	w	I (kA)	I/I_c (%)	H_w (T)	$H_{coil-max}$ (T)
Nb ₃ Sn	40	130	72	1.80	100	2.25	7.5
	40	120	72	1.67	85	2.10	7.0
	45	125	84	1.50	75	2.52	7.0
	50	140	84	1.67	85	3.05	7.0
NbTi	50	97	137	0.71	90	2.26	5.0

Relation between wiggler period and wiggler peak field on the beam axis for the Nb₃Sn wiggler.

Time evolution of the beam emittance



The time evolution of the horizontal and longitudinal emittances, relative energy spread, and bunch length for different wiggler fields at $L_w=152$ m ($C=364.96$ m). The red curves correspond to the wiggler peak field of 1.7 T and period length of 10 cm. The blue curves refer to the wiggler period length of 4.5 cm for the different wiggler fields



Taking into account IBS, the time span T_{eq} between the moment of the beam injection ($t=0$) and the moment when the size of the same beam reaches its equilibrium value is shown in the figure as a function of the wiggler peak field.

The minimum number of train pairs which can be accommodated in the ring to provide extraction of equilibrium beam with repetition rate f_{rr} is defined as

$$N_{2trains}^{\min} = f_{rr} T_{eq}$$

The maximum number of train pairs which can be accommodated in the ring with circumference C is defined as

$$N_{2trains}^{\max} = \frac{C}{T_{2trains}} = \frac{hc}{f_{rf} T_{2trains}}$$

$$T_{2trains} = 2(k_{bt} - 1)\tau_b + c \cdot 25.6 [ns] + \tau_k$$

τ_k is a gap between train pairs to allow a kicker to rise or fall for injection and extraction.

Assuming that the kicker's rise and fall times do not exceed 25 ns, the possible number of train pairs, which can be stored in the damping ring, is limited by

$$2 < N_{2trains} < 7$$

General lattice parameters.

Parameter	Symbol	RING 1	RING 2	RING 3	Unit
Energy	E	2.42	2.42	2.42	GeV
Circumference	C	364.96	364.96	300.48	m
Revolution time	T_0	1216.53	1216.53	1001.6	ns
Total length of wigglers	L_w	152	152	96	m
Number of wigglers	N_w	76	76	48	
Length of wiggler	L_{ID}	2	2	2	m
Wiggler peak field	B_w	1.7	2.52	2.52	T
Wiggler period length	λ_w	10	4.5	4.5	cm
Field of the bending magnet	B_a	0.932	0.932	0.932	T
Bending angle	θ	3.6°	3.6°	3.6°	
Length of the TME cell	L_{TME}	1.73	1.73	1.73	m
Number of the TME cell	N_{TME}	96	96	96	
Bending radius	ρ	8.67	8.67	8.67	m
Length of the bending magnet	L_θ	0.545	0.545	0.545	m
Energy loss per turn	U_0	2.0	3.96	2.63	MeV
Relative damping factor	F_w	4.65	10.22	6.45	
Horizontal damping time	τ_x	2.96	1.49	1.85	ms
Vertical damping time	τ_y	2.96	1.49	1.85	ms
Longitudinal damping time	τ_p	1.48	0.745	0.925	ms
Horizontal tune	ν_x	69.82	69.82	66.18	
Vertical tune	ν_y	33.7	33.7	30.23	
Horizontal natural chromaticity	$\partial\nu_x/\partial\delta$	-105.2	-103.4	-97.0	
Vertical natural chromaticity	$\partial\nu_y/\partial\delta$	-135.0	-139.1	-133.9	
Momentum compaction	α_p	0.807	0.782	0.972	$\times 10^{-4}$
RF frequency	f_{rf}	1875	1875	1875	MHz
RF wave length	λ_{rf}	0.16	0.16	0.16	m
RF peak voltage	V_{rf}	2250	4225	3030	kV
Harmonic number	h	2281	2281	1878	

Parameters* of the extracted beam.

Parameter	Symbol	RING 1	RING 2	RING 3	Unit
Bunch population	N_{bp}	2.56	2.56	2.56	$\times 10^9$
Bunches per train	k_{bt}	110	110	110	
Maximum number of bunch trains	N_{trains}^{max}	14	14	12	
Minimum number of bunch trains	N_{trains}^{min}	4	4	4	
Norm. horizontal emittance w/o IBS	$\gamma\epsilon_{x0}$	131	79	95	nm
Norm. horizontal emittance with IBS	$\gamma\epsilon_x$	540	380	430	nm
Norm. vertical emittance with IBS	$\gamma\epsilon_y$	3.4*	2.4*	2.7*	nm
Norm. longitudinal emittance** with IBS	ϵ_t	4990	4985	5000	eVm
RMS bunch length w/o IBS	σ_{s0}	1.21	1.25	1.21	mm
RMS energy spread w/o IBS	$\sigma_{\delta 0}$	0.915	0.113	0.111	%
RMS bunch length with IBS	σ_s	1.65	1.51	1.5	mm
RMS energy spread with IBS	σ_δ	0.125	0.136	0.137	%
Horizontal IBS growth time	T_x	3.89	1.88	2.34	ms
Longitudinal IBS growth time	T_p	5.57	4.403	4.83	ms

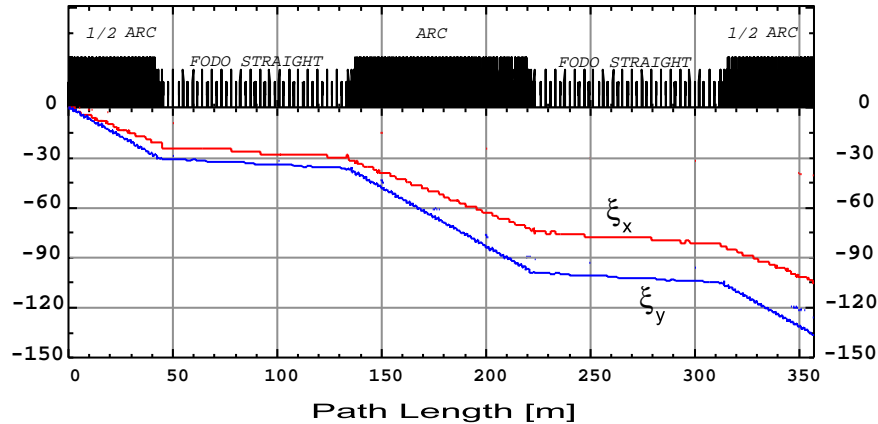
* Note that the parameters in this table were computed for the betatron coupling $\epsilon_{y0}/\epsilon_{x0} = 0.0063$ and zero vertical dispersion.

** Note that $\epsilon_t = \gamma\sigma_s\sigma_\delta m_0 c^2$.

In spite of the fact that the transverse emittances in the RING 1 design are larger than the transverse emittances in the RING 2 and RING 3 designs, the damping ring design RING 1 with the Nd-B-E permanent magnet wigglers is studied in details because a concrete design for the Nd-B-E permanent wiggler with period of 10 cm and field $Bw = 11.7$ was developed. In particular, the field map for this wiggler was known, which allowed detailed studies of the a nonlinear wiggler effect on the dynamic aperture. A tentative design of the superconducting NbSn wiggler was suggested only recently. For this reason, the superconducting wiggler scenarios were not studied in detail. In the following, we will, therefore, consider the damping ring design RING 1.

Natural chromaticity of the damping ring

$$\xi_x = -105.2 \text{ and } \xi_y = -135$$



The horizontal ξ_x and vertical natural chromaticity ξ_y along the CLIC damping ring

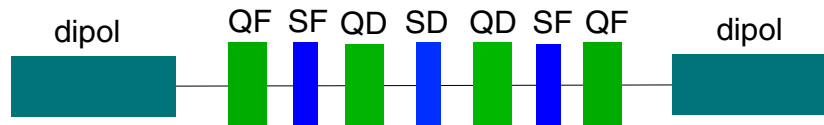
A sextupole scheme for the TME structure

For the damping ring a localized correction is not possible since, it comprises two dispersion-free long straight sections. In this case, the natural chromaticity produced in the straight sections have to be corrected only by sextupoles inserted in the arcs.

- To perform an efficient correction of the ξ_x , the sextupoles with $K_2 > 0$ have to be inserted in the places where the β_x functions have a high value and $\beta_y \ll \beta_x$.
- To correct ξ_y efficiently, the sextupoles with $K_2 < 0$ have to be inserted at positions where the β_y functions have high values and $\beta_x \ll \beta_y$.
- To minimize the sextupole strengths, it is important to place them at positions where D_x is as high as possible and the betatron functions have a good split.

the sextupoles introduce nonlinearities which are defined by

- the second-order chromatic aberration related with $(D\delta)^2$
- the geometrical aberrations (geometrical terms) proportional to $(x^2 - y^2)$ and xy .



! due to the small beta and dispersion functions in the arc =>
strong sextupoles are needed that consequently limits the
dynamic aperture

! In order to maximize the dynamic aperture, the nonlinearities
induced by sextupoles must be minimized

First order sextupole [+quadrupole] Hamiltonian

- 2 phase independent terms \rightarrow chromaticities:

$$h_{11001} = +J_x \delta \left[\sum_n^{N_{sext}} (2b_3 L)_n \beta_{xn} D_n - \sum_n^{N_{quad}} (b_2 L)_n \beta_{xn} \right] \rightarrow \xi_x$$

$$h_{00111} = -J_y \delta \left[\sum_n^{N_{sext}} (2b_3 L)_n \beta_{yn} D_n - \sum_n^{N_{quad}} (b_2 L)_n \beta_{yn} \right] \rightarrow \xi_y$$

- 7 phase dependant terms \rightarrow resonances: \implies

$$a_x = (j - k) \quad a_y = (l - m)$$

$$h_{21000} = h_{12000}^* \longrightarrow Q_x$$

$$h_{30000} = h_{03000}^* \longrightarrow 3Q_x$$

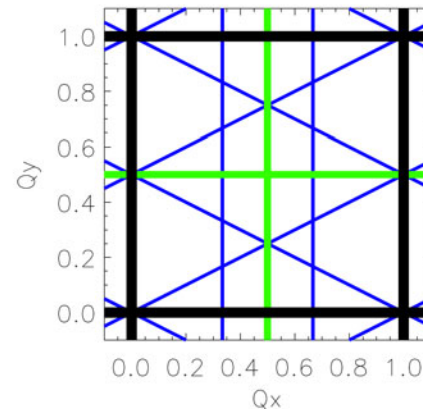
$$h_{10110} = h_{01110}^* \longrightarrow Q_x$$

$$h_{10200} = h_{01020}^* \longrightarrow Q_x + 2Q_y$$

$$h_{10020} = h_{01200}^* \longrightarrow Q_x - 2Q_y$$

$$h_{20001} = h_{02001}^* \longrightarrow 2Q_x$$

$$h_{00201} = h_{00021}^* \longrightarrow 2Q_y$$



Second order sextupole [+first order octupole] Hamiltonian

$$\sum_n \sum_m (b_3 L)_n (b_3 L)_m \times (\beta_n, \phi_n \beta_m, \phi_m \dots) + \left[\sum_q (b_4 L)_q \times (\beta_q, \phi_q \dots) \right]$$

- **3 phase independant terms** → **amplitude dependant tune shifts:**

$$\frac{\partial Q_x}{\partial J_x} \quad \frac{\partial Q_x}{\partial J_y} = \frac{\partial Q_y}{\partial J_x} \quad \frac{\partial Q_y}{\partial J_y}$$

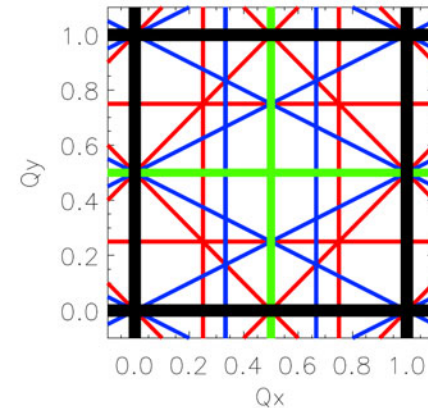
- **2 phase independant off-momentum terms** → **second order chromaticities:**

$$\xi_{x/y}^{(2)} = \frac{\partial^2 Q_{x/y}}{\partial \delta^2}$$

- **8 phase dependant terms**

→ **octupolar resonances:**

$h_{40000} \rightarrow 4Q_x$	$h_{31000} \rightarrow 2Q_x$
$h_{00400} \rightarrow 4Q_y$	$h_{20110} \rightarrow 2Q_x$
$h_{20200} \rightarrow 2Q_x + 2Q_y$	$h_{00310} \rightarrow 2Q_y$
$h_{20020} \rightarrow 2Q_x - 2Q_y$	$h_{01110} \rightarrow 2Q_y$



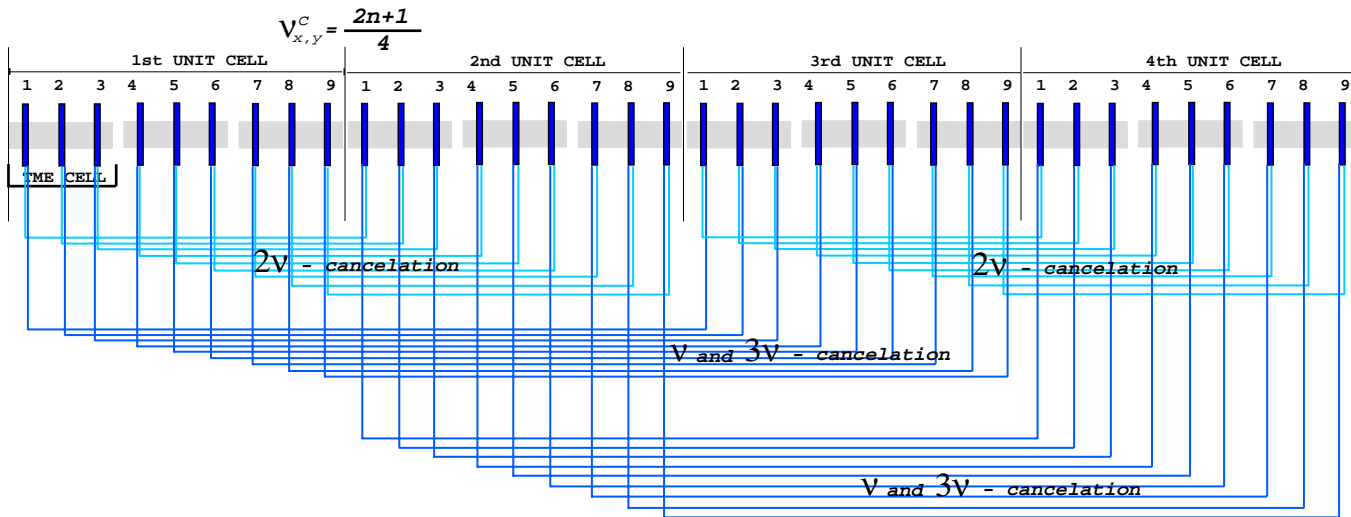
Conditions for the second order sextupolar achromat configuration:

Consider an achromat built from of N identical cells of length l and with tunes per cell ν_x^c and ν_y^c . For any second order achromat the total tunes must be

$$N\nu_x^c = \text{integer}, \quad N\nu_y^c = \text{integer}$$

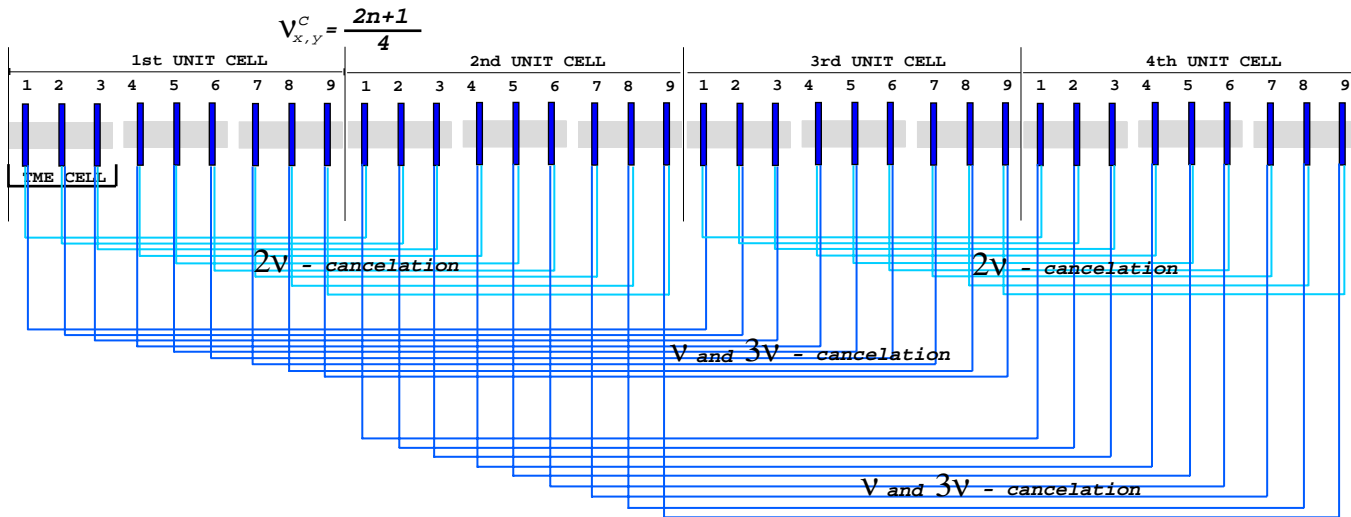
unperturbed tunes ν_x^c and ν_y^c must avoid the following resonance

$$n_x\nu_x^c + n_y\nu_y^c \neq \text{integer}$$



High periodicity of the arc allows for the following variant of the second order sextupolar achromat configuration:

- Phase advances of the TME cell $NU_x = 0.5833$ and $NU_y = 0.25$
- The achromat unit cell consists of 3 TME cells where sextupoles with different strengths are located.
- Repeating the unit cell 4 times, we arrange the second order sextupolar achromat that meets requirements stated above with overall phase advance $\Delta\mu_{xa} = 7 \times 2\pi$
 $\Delta\mu_{ya} = 3 \times 2\pi$
- Nine sextupole families can be used in such achromat configuration

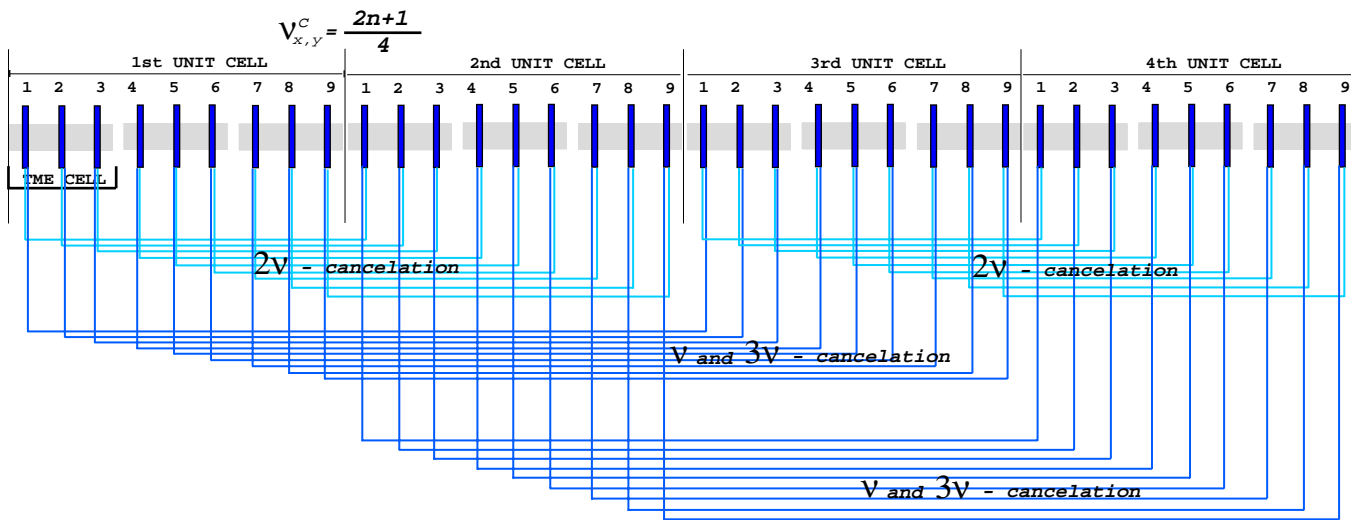


- The sextupoles in the first and second unit cells constitute - I transformers with the sextupoles located in the third and fourth unit cells respectively, =>

$$\nu_x, 3\nu_x, \nu_x - 2\nu_y, \nu_x + 2\nu_y \quad \text{cancellation}$$

- The phase advances over the unit cell $\Delta\mu_x^c = 1.75 \times 2\pi$ and $\Delta\mu_y^c = 0.75 \times 2\pi$

$$2\nu_x, 2\nu_y, 2\nu_x + 2\nu_y, 2\nu_x - 2\nu_y \quad \text{cancellation}$$

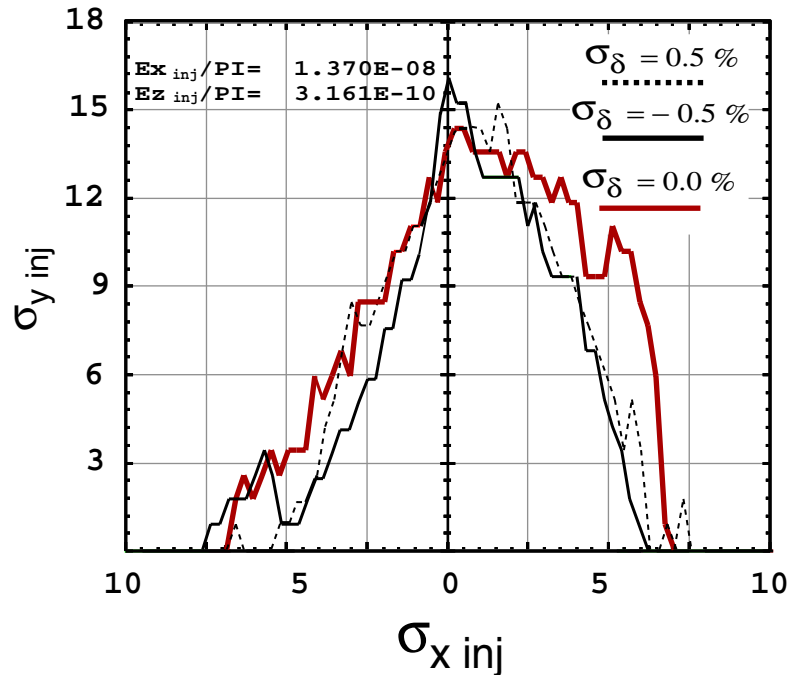


Using BETA-LNS code, we optimized the strength of sextupoles to compensate natural chromaticity and to minimize 5 constraints

$$\frac{\partial \nu_x}{\partial J_x} = 0, \quad \frac{\partial \nu_x}{\partial J_y} = \frac{\partial \nu_y}{\partial J_x} = 0, \quad \frac{\partial \nu_y}{\partial J_y} = 0, \quad \frac{\partial^2 \nu_x}{\partial \delta^2} = 0, \quad \frac{\partial^2 \nu_y}{\partial \delta^2} = 0$$

However It was complicated to find a zero solution for all constrains even when assigning significant weight factors for "stiff constrains", because the arc lattice is highly symmetric.

In our consideration we quote the dynamic aperture in terms of sigma of the injected beam size with horizontal and vertical normalized emittances of 63 um and 1.5 um, respectively.



Review of wiggler magnet technologies

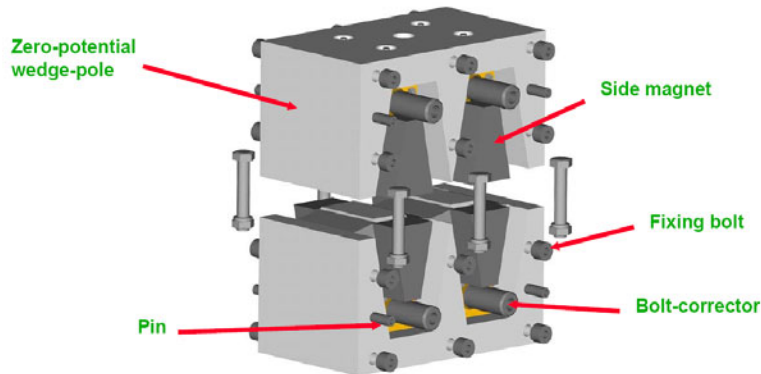
Wiggler magnet technologies for producing a high field with short period.

Technology	Advantages	Disadvantages
Electromagnet	Field tuning flexibility; Radiation hardness; Field stability	Power consumption; Low field (< 1.7 T) at short wiggler period (7-10 cm)
Pure Permanent Magnet	Does not require power; Short wiggler period (7-10 cm)	Radiation damage; Field varies with temperature; No field tuning flexibility; Weak max field (< 1.7 T)
Hybrid Permanent Magnet (combination of permanent magnet blocks and high saturation steel)	Does not require power; Short wiggler period; Magnetic field > 1.7 T can be achieved	Radiation damage; Field varies with temperature; No field tuning flexibility
Hybrid Electromagnet (combination of electromagnets & permanent magnets)	Temperature stability better than for PPM; Field tuning flexibility (typically about 25 %); Magnetic field > 1.7 T can be achieved	Radiation damage;
Superconducting	High field at short wiggler period; Field stability	Cryogenic infrastructure

NdFeB permanent magnet damping wiggler

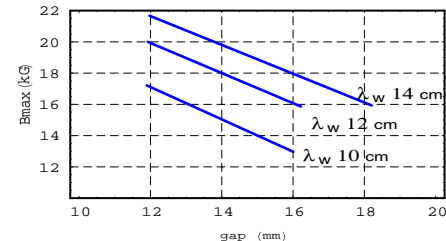
A tentative design of the NdFeB permanent wiggler for the CLIC damping ring is based on the wiggler design for the PETRA-3 ring. The parameters of the PETRA-3 wiggler¹ (wiggler period, gap, field amplitude) were re-optimized to meet CLIC damping ring requirements.

An optimized design of the NdFeB permanent wiggler for the CLIC damping ring is shown in the Figure and the corresponding wiggler parameters are summarized in the Table.



One period of the NdFeB wiggler

Field amplitude	1.7 T
Period of the wiggler	10 cm
Number of periods	20
Magnetic gap of the wiggler	12 mm
Pole width	60 mm
Magnet material	Nd-Fe-B
Pole material	Vanadium
	Permendur



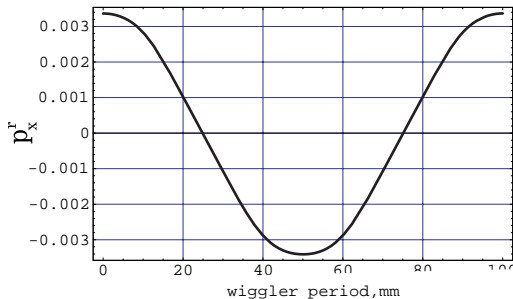
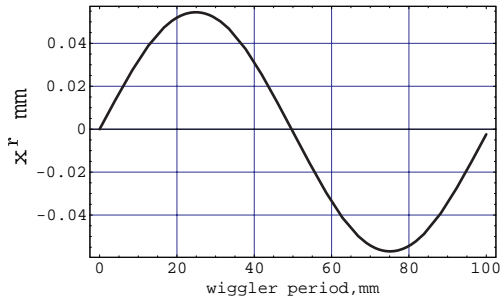
Peak field amplitude vs. pole gap for different wiggler periods

¹ P. Vobly, "Magnetic field calculation and design optimization of the wigglers for CLIC dumping ring," Report on the WIGGLE 2005 Mini-Workshop, INFN-LNF, Frascati 21-22 February, 2005

Tracking result

The use of NdFeB permanent magnet wigglers does not lead to a reduction of the dynamic aperture when the sextupoles are turned on.¹

With nonlinearities induced only by wigglers (if the sextupoles are turned off), the dynamic aperture is much larger than the physical aperture of the vacuum chamber of the machine.



Reference orbit for the one wiggler period

¹ M. Korostelev, F. Zimmermann, "CLIC Damping Ring Optics Design Studies", PAC 2005 - Proceedings

SR power and absorption

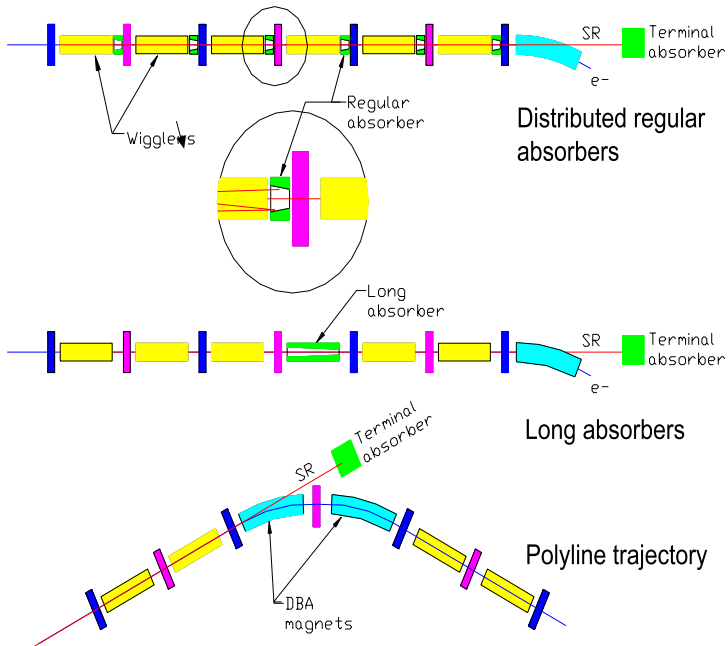
An effective collimation system in the wiggler straight sections is very important. Because of the large synchrotron radiation power an interception strategy has to be studied. A HPM wiggler would require upstream collimation to limit the radiation within the straight wiggler sections. The parameters of synchrotron radiation from the HPM NdFeB wiggler are summarized in the Table below.

Radiation power for $B_w = 1.7$ T and $\lambda_w = 10$ cm.

Deflection parameter K	$K = 0.934\lambda_w[cm]B_w[T]$	15.88
Wiggler length	L_{ID}	2 m
Average beam current	$I[A] = N_t k_{bt} N_{bp} 1.6 \times 10^{-19} / T_0 [sec]$	0.52 A
Tot.power from one wiggler	$P_T[kW] = 0.633E^2[GeV]B_w^2[T]L_{ID}[m]I[A]$	11.18 kW
Relativistic factor	$\gamma = E/m_e c^2$	4743
Vertical divergence angle	$\theta_v = \gamma^{-1}$	0.21 mrad
Horizontal divergence angle	$\theta_h = 2K/\gamma$	6.69 mrad
Tot.power from 38 wigglers	$P_A[kW] = 38P_T$	424.8 kW

The average beam current of 0.52 A corresponding to the maximum number of bunch trains $N_t=14$ which can be stored in the damping ring. The SR power generated by one wiggler module with length of 2 m is equal to 11.18 kW. Taking into account that the damping ring includes 76 wigglers in the two straight sections, the total radiation power from all wigglers is equal to 849.6 kW.

Three possible approaches for the absorption of SR power in the damping ring can be applied

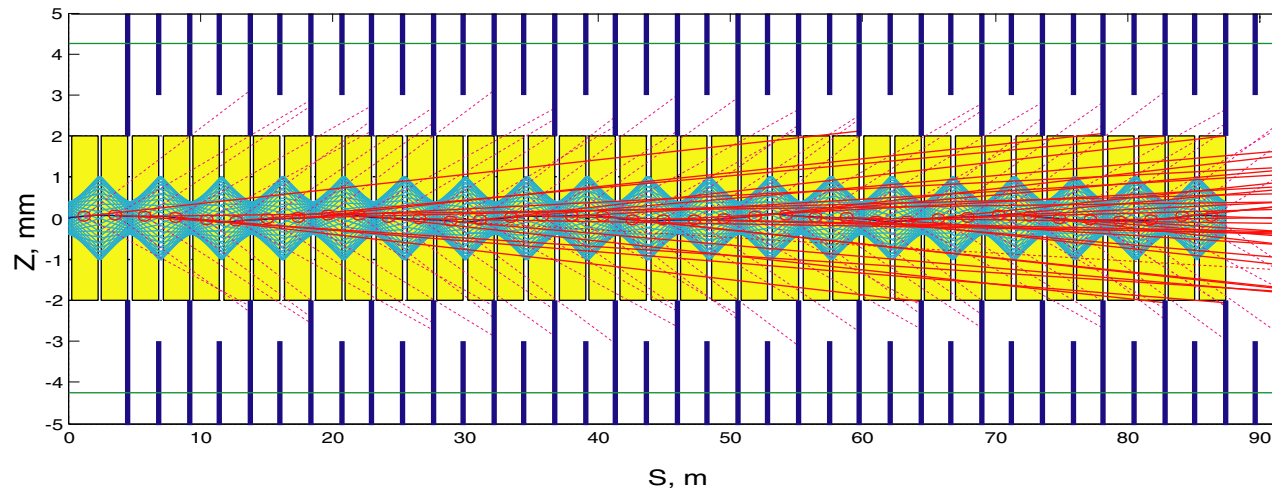


The main disadvantage of the third method (polyline trajectories) is that a few small achromatic bends of beam trajectory, provided for example by DBA cell in the dispersion free straight section, are needed to let out the radiation to an absorbers.

Using several long absorbers which can be placed instead of some wigglers, results in overheating of the vacuum chamber between neighbouring long absorbers and also yields a big power of SR at the terminal absorber. If the 12th, 24th and 36th wiggler are replaced by a long absorber, than integrated value of SR power deposited on the vacuum chamber is about 600 W/m which is not acceptable.

From our point of view, the regularly distributed small absorbers is the more preferable variant, though it still leads to quite significant power in the terminal absorber.

An absorber in front of defocusing quadrupoles has the vertical/horizontal aperture equal to **6/60 mm**, but the vertical/horizontal aperture of absorbers located in front of focusing quadrupoles is **4/60 mm**, as it is sketched in the figure below.



SR power loads on wiggler vacuum chambers and regularly distributed copper absorbers were simulated for the closed orbit distortion of 100 μm .

Such configuration of regularly distributed absorbers ensures the absorption of **334.5 kW** of SR power per straight section, for an average current of 0.52 A. The rest of the SR power, **90.3 kW**, will be taken up by a terminal absorber placed at the end of the straight section. On average, the absorbers with vertical aperture of 4 mm and 6 mm absorb **13.4 kW** and **4.2 kW** of SR power, respectively. Only a small fraction of SR power hits the vacuum chamber. Its integrated value over the vacuum chamber of the straight section is equal to **6 W/m** for the closed orbit distortion of 100 μm .

3 types of error sources which increase the vertical emittance via the betatron coupling C_β or the vertical dispersion D_y :

1. Transverse quadrupole misalignments, dipole errors and their effects:

Dipolar tilt errors --> D_y

Dipolar correctors --> D_y

Vertical closed orbit (CO) in quadrupoles --> D_y

Vertical CO in sextupoles --> D_y, C_β

2. Sextupole misalignments and their effects:

Vertical sextupole displacements --> D_y, C_β

Vertical CO in sextupoles --> D_y

3. Quadrupole tilt errors:

Skew quadrupoles --> D_y, C_β

Vertical emittance increase due to random errors

The vertical emittance from uncorrelated sextupole misalignments may be written

$$\epsilon_{y0} = \langle \Delta Y_{\text{sext}}^2 \rangle \left[\Sigma_{K2}^{\beta} \frac{J_x(1 - \cos 2\pi\nu_x \cos 2\pi\nu_y)}{4J_y(\cos 2\pi\nu_x - \cos 2\pi\nu_y)^2} \epsilon_x + \Sigma_{K2}^D \frac{J_e \sigma_{\delta}^2}{4 \sin^2 \pi\nu_y} \right],$$

and the vertical emittance from uncorrelated quadrupole rotations may be written

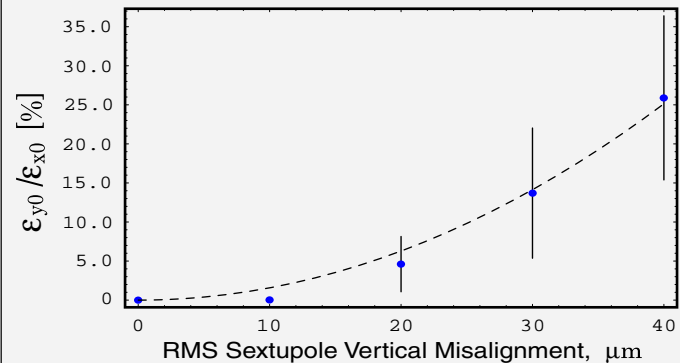
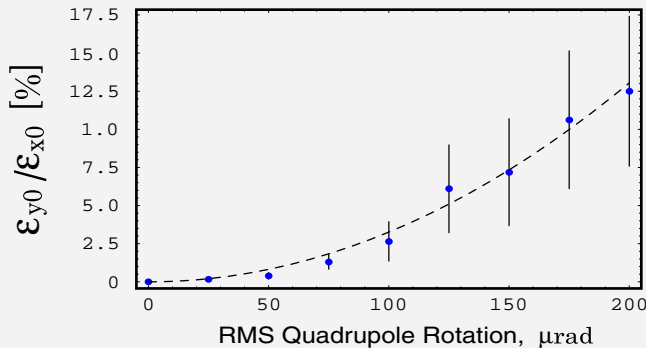
$$\epsilon_{y0} = \langle \Delta \Theta_{\text{quad}}^2 \rangle \left[\Sigma_{K1}^{\beta} \frac{J_x(1 - \cos 2\pi\nu_x \cos 2\pi\nu_y)}{J_y(\cos 2\pi\nu_x - \cos 2\pi\nu_y)^2} \epsilon_x + \Sigma_{K1}^D \frac{J_e \sigma_{\delta}^2}{\sin^2 \pi\nu_y} \right],$$

$$\Sigma_{K2}^{\beta} = \sum_{\text{sext}} \beta_x \beta_y (K_2 l)^2,$$

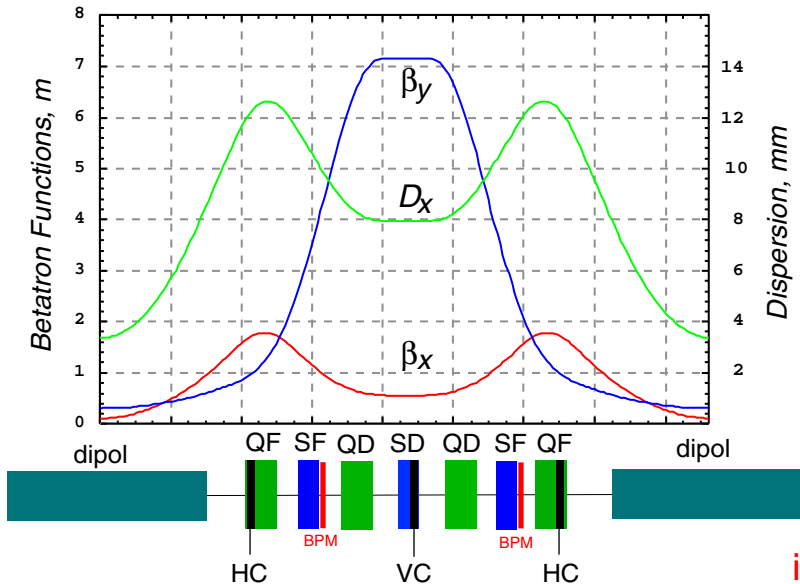
$$\Sigma_{K2}^D = \sum_{\text{sext}} \beta_y (K_2 l D_x)^2$$

$$\Sigma_{K1}^{\beta} = \sum_{\text{quad}} \beta_x \beta_y (K_1 l)^2$$

$$\Sigma_{K1}^D = \sum_{\text{quad}} \beta_y (K_1 l D_x)^2$$



In the simulations, the random errors were generated with gaussian distributions truncated at ± 3 sigma



we arranged the horizontal correctors HC as additional coils in the focusing quadrupoles QF, where β_x is maximum and the vertical correctors VC are set as additional coils in the SD sextupoles of the arcs.

the vertical and horizontal beam position is simultaneously detected by each BPM

BPM and dipole corrector are installed near each quadrupole of the FODO straight section

in total: 246 HC, 146 VC, 292 BPM

- The correctors **HC** with vertical dipole field that provide a horizontal kick and BPMs which are selected to detect the horizontal orbit displacement have to be located at places where the horizontal beta function is maximum.
- The correctors **VC** with horizontal dipole field that provide a vertical kick and BPMs which are selected to detect the vertical orbit displacement have to be installed at places where the vertical beta function is maximum.
- To minimize D_y skew quadrupole correctors should be installed in the arc at positions where the horizontal dispersion D_x is largest.

simultaneous correction of the orbit and the dispersion by dispersion free steering (DFS) method using the dipole correctors

after correction at $\langle \Delta Y_{\text{quad}} \rangle = \langle \Delta X_{\text{quad}} \rangle = 90 \mu\text{m}$

normalized zero-current vertical emittance **< 2.2 nm**

after correction at $\langle \Delta Y_{\text{quad}} \rangle = \langle \Delta X_{\text{quad}} \rangle = 90 \mu\text{m}$ and

$\langle \Delta Y_{\text{sext}} \rangle = \langle \Delta X_{\text{sext}} \rangle = 20 \mu\text{m}$

normalized zero-current vertical emittance **~ 10 nm**

Skew quadrupole correction of vertical dispersion and betatron coupling

In the CLIC damping ring, the dominant contribution to the emittance after closed-orbit distortion (COD) correction is the vertical dispersion.

Skew quadrupole correctors are inserted as additional coils into each second sextupole SD. Thus, 48 units of the skew correctors are included in the damping ring. The standard deviations of random errors assigned for the simulations of the correction are listed in the Table below. Note that in these simulations the random errors are generated with Gaussian distributions truncated at 2σ .

Random alignment errors assigned to the CLIC damping ring.

Imperfections	Symbol	1 r.m.s.
Quadrupole misalignment	$\langle \Delta Y_{\text{quad}} \rangle, \langle \Delta X_{\text{quad}} \rangle$	90 μm .
Sextupole misalignment	$\langle \Delta Y_{\text{sext}} \rangle, \langle \Delta X_{\text{sext}} \rangle$	40 μm
Quadrupole rotation	$\langle \Delta \Theta_{\text{quad}} \rangle$	100 μrad
Dipole rotation	$\langle \Delta \Theta_{\text{dipole arc}} \rangle$	100 μrad .
BPMs resolution	$\langle R_{\text{BPM}} \rangle$	2 μm .

The BETA-LNS code enables one to choose a weight factors for minimization of the betatron coupling and vertical dispersion

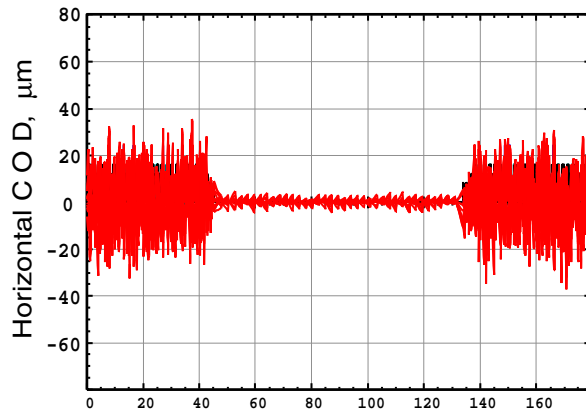
Beam parameters after correction

Taking into account IBS, the equilibrium emittances, rms bunch length and rms energy spread after the dipole and skew quadrupole correction are the following:

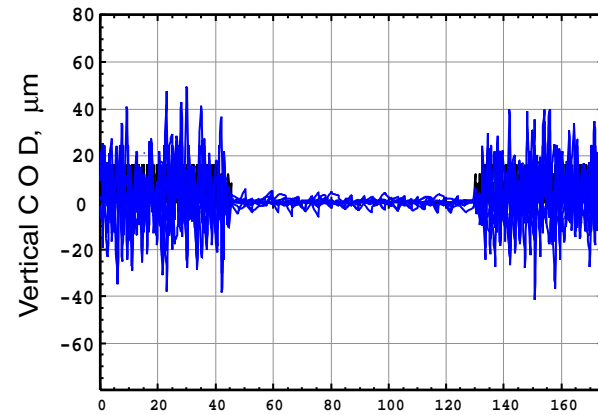
- Horizontal emittance $\langle \gamma \epsilon_x \rangle$: 530 nm
- Vertical emittance $\langle \gamma \epsilon_y \rangle$: 3.3 nm
- Emittance ratio $\langle \epsilon_y / \epsilon_x \rangle$: 0.62 %
- RMS bunch length $\langle \sigma_s \rangle$: 1.63 mm
- RMS energy spread $\langle \sigma_p \rangle$: 12.35×10^{-4}
- Longitudinal emittance $\langle \gamma m_e c^2 \sigma_p \sigma_s \rangle$: 4892 eVm

The vertical emittance ϵ_{y0} after correction is shared as

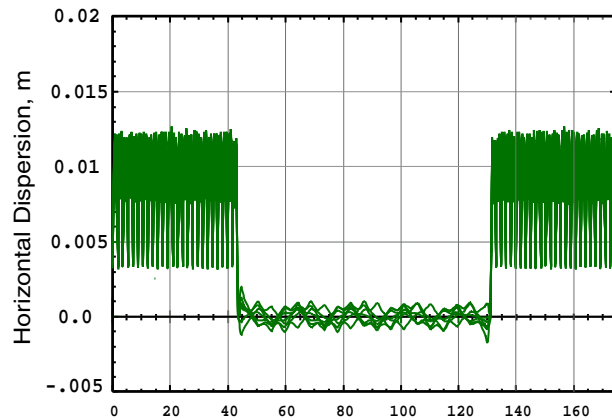
- contribution of betatron coupling $\epsilon_{y0,\beta}$: 8 % of ϵ_{y0}
- contribution of spurious vertical dispersion $\epsilon_{y0,d}$: 92 % of ϵ_{y0}



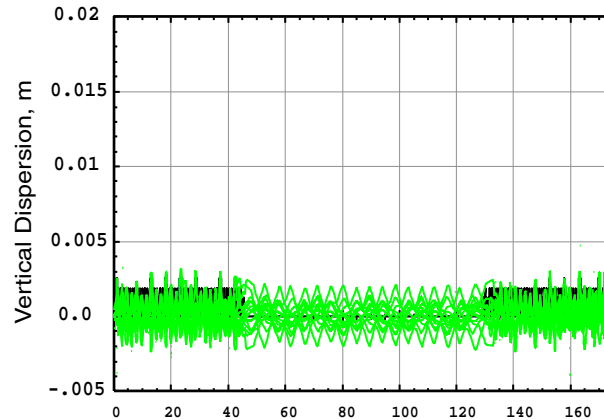
Half of the damping ring circumference, (m)



Half of the damping ring circumference, (m)



Half of the damping ring circumference, (m)



Half of the damping ring circumference, (m)

Dynamic aperture

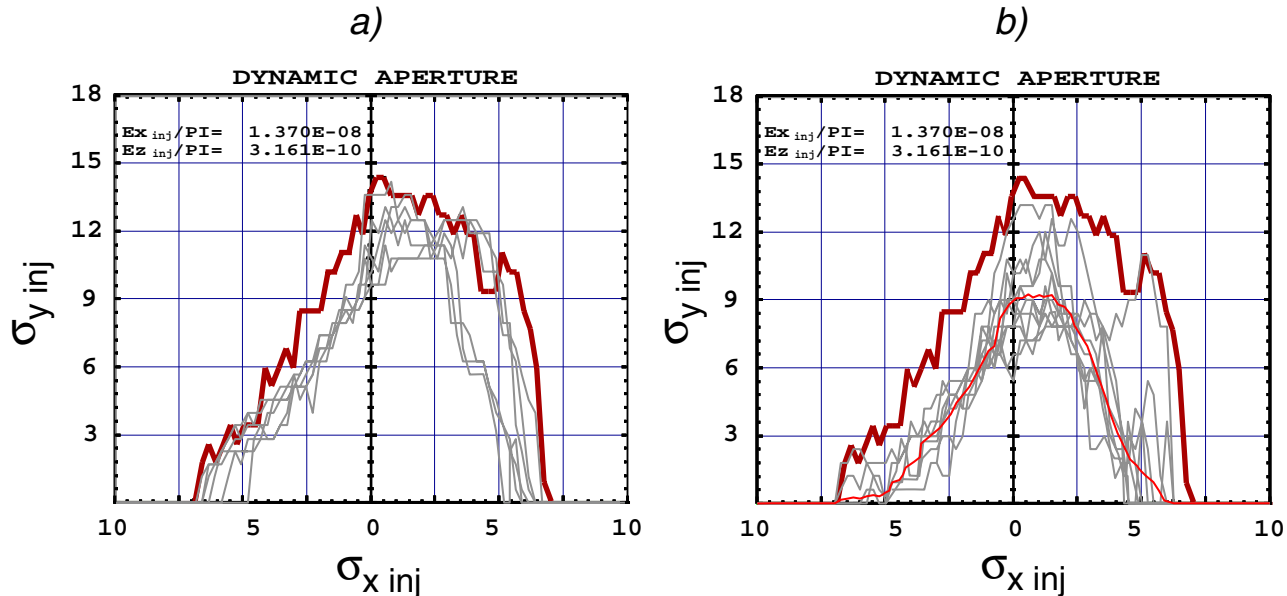


Figure 7.13: a) Dynamic aperture of the damping ring after dipole correction carried out in the presence of quadrupole misalignments only, with $\langle \Delta Y_{\text{quad}} \rangle = \langle \Delta X_{\text{quad}} \rangle = 90 \mu\text{m}$. The thick solid line shows the dynamic aperture without errors; b) Dynamic aperture of the damping ring after dipole and skew quadrupole correction carried out in the presence of all alignment errors listed in Table 7.1. The red thin line corresponds to the mean value of the dynamic aperture.

Longitudinal and Transverse Micro-Wave Instability

For $b > \sigma_z$, the Keil-Schnell-Boussard threshold is

$$\frac{Z_{\parallel}}{n} = Z_0 \sqrt{\frac{\pi}{2}} \frac{\gamma \alpha_p \sigma_{\delta}^2 \sigma_s}{N_{bp} r_0} \left(\frac{b}{\sigma_s} \right)^2 = 2.87 \Omega ,$$

This threshold is 3 - 14 times higher than expected impedance of the CLIC damping ring scaled from KEKB LER

There is also a transverse coasting-beam instability associated with the transverse impedance. Again applying the Keil-Schnell-Boussard criterion, the threshold for this instability may be written:

$$Z_{\perp} = Z_0 \frac{\gamma \alpha_p \sigma_{\delta} \sigma_s \nu_y}{N_{bp} r_0} \frac{\omega_0}{C} = 19.4 \text{ M}\Omega/\text{m} ,$$

Space Charge

Space-charge forces lead to a significant vertical tune shift, because of the large circumference and small vertical beam size. The incoherent space charge tune shift is

$$\Delta\nu_y^{sc} = \frac{N_{bp}r_0}{(2\pi)^{3/2}\gamma^3\sigma_s} \int_0^C \frac{\beta_y}{\sigma_y(\sigma_x + \sigma_y)} ds \approx 0.1 ,$$

close to the maximum acceptable value

Coherent Synchrotron Radiation

Coherent synchrotron radiation is benign, causing only a 5% bunch lengthening without instability.

Electron Cloud

-Simulated electron densities in the wiggler vary between 10^{13} m^{-3} and several 10^{14} m^{-3} , which is to be compared with a simulated single-bunch instability threshold of about $2 \times 10^{12} \text{ m}^{-3}$.

Potential limitations to be addressed are the high electron-cloud densities in the wiggler sections and the fast beam-ion instability. Possible remedies include clearing electrodes and photon stops for the wiggler, and an improved vacuum.

Ion Instabilities

For the CLIC damping ring we assume a total pressure of 1 nTorr (1.3×10^{-7} Pa). This pressure is roughly consistent with the best values achieved at the KEK/ATF and with typical pressures at the KEKB HER. We also assume that 20% of this vacuum pressure is due to carbon monoxide (CO), the rest being dominated by hydrogen. We have only considered the ions produced during the passage of a single train. To avoid ion accumulation between trains, the inter-train gap must be larger than

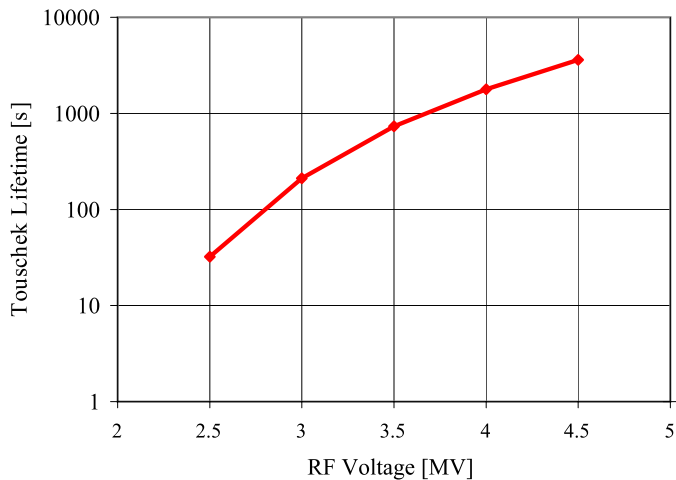
$$L_{g,cl} \approx 10 \times c / (\pi f_i),$$

The resulting analytical estimates are compiled in the Table, invoking an ionization cross section for CO molecules of 0.2 nTorr, and a 30% relative ion-frequency spread.

Parameter	CLIC	
	Arc	Wiggler
Critical mass, A_{crit}	15	9
Vertical ion frequency [MHz]	360	275
Minimum gap, $L_{g,cl}$ [m]	2.7	3.5
Ion density ρ_{ion} [cm^{-3}]	0.58	0.34
Exponential rise time at train end [μs]	189	185 [av. rise t. 187]
Incoherent tune shift at train end ΔQ_y	0.001	0.001 [total 0.0026]

For operating regime with 14 stored bunch trains, a gap between trains in the CLIC damping ring is not less than 7.5 m.

Touschek Lifetime



The Touschek lifetime can be computed using the Piwinski formalism, including horizontal and vertical dispersion, which was implemented in the MAD-X programme. The figure illustrates how the Touschek lifetime varies with the ring rf voltage, even for an rf voltage as low as 2.5 MV, the Touschek lifetime is much longer than the bunch-train store time of 13.3 ms.

Resistive Wall Instability

The dominant transverse impedance source is the resistive wall in the long wiggler sections with only about 8 mm vertical half aperture. The classical growth rate of the most unstable mode is estimated as

$$\frac{1}{\tau_{rw}} \approx \frac{1}{2} \frac{\pi^2}{8} \frac{\beta_y N_{bp} h r_0 c^2}{2\pi b_w^3 \gamma \sqrt{\sigma c C}} \frac{1}{\sqrt{|Q - n|}} \approx 1854 \text{ s}^{-1},$$

corresponds to about 500 turns.

Summary

- With imperfections, the correction system restores the vertical and horizontal emittances to the values 3.4 nm and 540 nm, respectively (taking into account IBS).
- A dynamic aperture of 5 sigma horizontally and 9 sigma vertically in terms of injected beam size is obtained after the correction.
- The nonlinearities introduced by the NdFeB wigglers do not lead to a reduction of the dynamic aperture.
- The effective collimation system to absorb SR was developed.
- Electron-cloud effect is critical. Other among of collective effects are not critical.